CONF-75-189-E
E-0311, E-0002
C75/08/27

Expt #311

Paper Presented at the
1975 Division of Particles and Fields
American Physical Society Meeting
Seattle, Washington, August 27-29

NATIONAL ACCELERATOR LAB.
OCT 21 1975
PROGRAM PLANNING OFFICE

Multiplicities and Inclusive and Exclusive Reactions at Fermilab Energies

J. Whitmore*
Michigan State University, E. Lansing, Mich. 48824

ABSTRACT

Some new data on $\bar{p}p$ multiplicities are discussed and comparisons are made with lower energy annihilation data. A summary of inclusive single particle production includes a discussion of $\pi^{\pm}$ production in 100 GeV/c $\bar{p}p$ interactions and a comparison of $\pi^{\pm}$ production in the target and beam fragmentation regions. New data on leading particle clusters and ρ° production are presented. The discussion of the exclusive 4 and 6-body final states in $\pi^{-}p$ and pp interactions centers on the questions of the existence of double pomeron exchange and double diffractive excitation.

I. 100 GeV/c $\bar{p}p$ Interactions

Recently, data have been acquired from 100 GeV/c $\bar{p}p$ interactions. Among the first results obtained[1] from these data are charged multiplicity cross sections and the moments of the multiplicity distribution. Preliminary results and a discussion of the elastic $\bar{p}p$ scattering have been presented elsewhere[2]. Figure 1 shows $\langle n \rangle$, the average charged multiplicity, and the ratio of $\langle n \rangle / D$, when $D = [\langle n^2 \rangle - \langle n \rangle^2]^{1/2}$, for $\bar{p}p$ and pp data as a function of the incident momentum (and s, the cm energy squared). Figure 1a shows that the $\bar{p}p$ charged multiplicity is about 0.5 greater than that for pp interactions at the same energy and shows no indication of approaching the pp values. Figure 1b suggests that the $\bar{p}p$ values of $\langle n \rangle / D$ at high energies may be increasing above the value of 2 for the pp data.

To investigate the difference between $\bar{p}p$ and pp in more detail, Fig. 2 shows a compilation of total annihilation cross sections as a function of the incident $\bar{p}$ momentum and a comparison with the difference in $\bar{p}p$ and pp total cross sections[3]. The straight line is a fit[3] to p_{Lab}^{-n} with $n = 0.61 \pm 0.02$ and is an excellent representation of both sets of data over two orders of magnitude in s. The good agreement between the annihilation data and the ($\bar{p}p$-pp) difference motivates Fig. 3 in which are shown various moments of the multiplicity distribution for pp and $\bar{p}p$ annihilation data for $s \leq 20$ GeV^2. Shown as the open circles in Fig. 3 are the moments estimated[4] by using the inelastic topological cross section differences, $\sigma_n(\bar{p}p) - \sigma_n(pp)$, for $P_{Lab} = 12$, 15, 22, 32 and 100 GeV/c. One observes (Fig. 3a) that the negative charged particle multiplicity, as <u>estimated</u> by taking the difference ($\bar{p}p$-pp) is in excellent agreement with a smooth extrapolation of the <u>measured</u> $\bar{p}p$

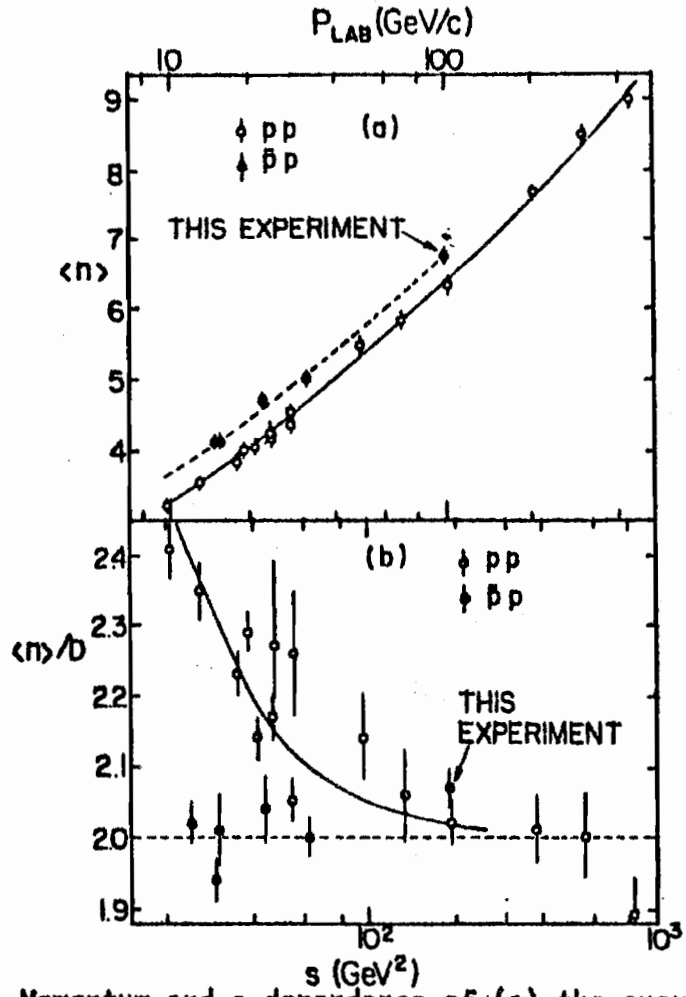

Fig. 1. Momentum and s dependence of (a) the averaged charged multiplicity, <n>, and (b) the ratio of <n> to dispersion, D, for p̄p and pp interactions. The curves are to guide the eye.

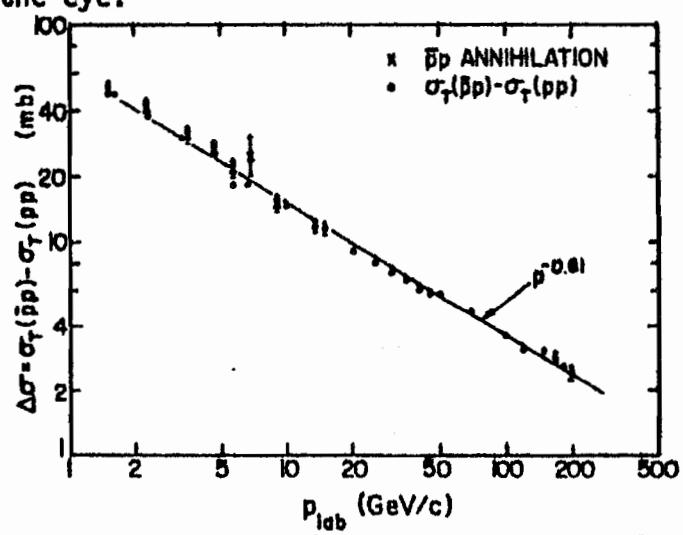

Fig. 2. Differences in total cross section for p̄p and pp interactions as a function of the incident beam momentum. Also shown are the total annihilation cross sections.

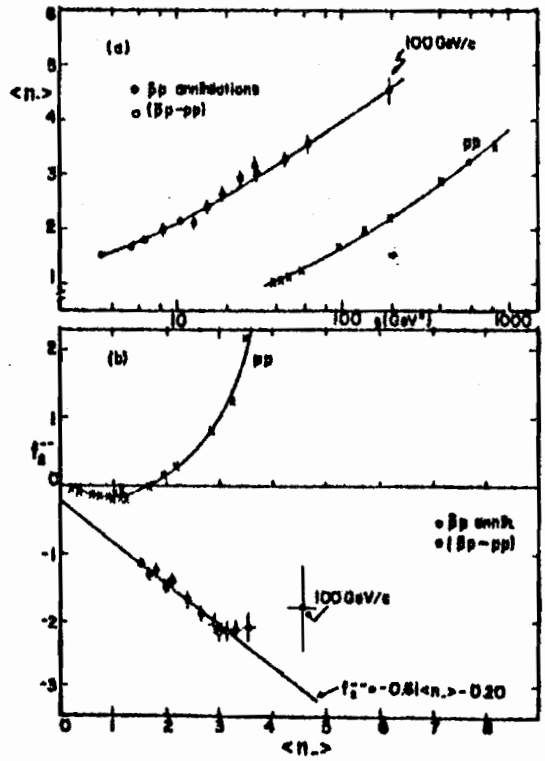

Fig. 3 (a) Energy dependence of the mean negative multiplicity, $\langle n_- \rangle$, for $\bar{p}p$ annihilations and pp data. (b) f_2^{--} versus $\langle n_- \rangle$ for $\bar{p}p$ annihilations and pp inelastic data. Also shown are estimates of ($\bar{p}p$-pp) at high energy.

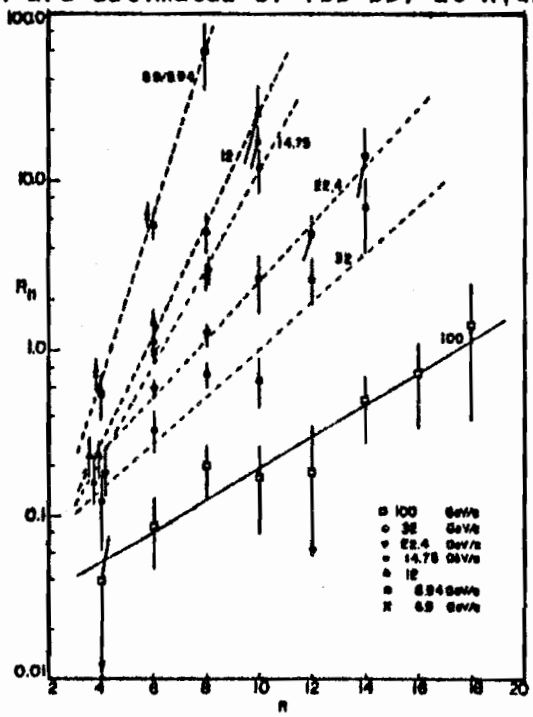

Fig. 4. R_n (see text) versus n for $\bar{p}p$ and pp data. The straight lines are fits to the form $R_n = A\beta^n$ at each momentum.

annihilation data. Furthermore, the 2 unit difference between $\langle n_- \rangle$ for $\bar{p}p$ annihilations and for inelastic pp interactions appears constant over a wide range of s. Figure 3b shows $f_2^{--} = \langle n_-(n_--1)\rangle - \langle n_-\rangle^2$ as a function of $\langle n_-\rangle$. The high energy estimates[4] from ($\bar{p}p$-pp) once again continue smoothly from the low energy annihilation data. The expression $f_2^{--} = -0.61\langle n_-\rangle - 0.20$ results from a fit to the data and is in excellent agreement with a single cluster formation model for the annihilation process[5]. The pp data at high energies have a positive value of f_2^{--}. This can be understood as a consequence of producing more than one cluster[5]. There is perhaps a suggestion of similar behavior occurring in the annihilation data for $P_{Lab} \gtrsim 30$ GeV/c.

Figure 4 shows[4] the values of $R_n = [\sigma_n(\bar{p}p) - \sigma_n(pp)]/\sigma_n(pp)$ as a function of n for data between $P_{Lab} = 6.9$ and 100 GeV/c. The straight line fits of the form $R_n = A\beta^n$ are excellent representations of these data. The values[4] of $\alpha \equiv -\ell nA/\ell ns$ and β are plotted in Fig. 5 as a function of ℓns. There is evidence that both parameters are approaching asymptotic values. (At 100 GeV/c, $\alpha = 0.73 \pm 0.04$ and $\beta = 1.24 \pm 0.02$.) This suggests that at high energies $R_n = s^{-\alpha}\beta^n$, in agreement with a suggestion of Eylon and Harari who predicted[6] that

$$R_n = \beta^n s^{2\alpha_B - 2\alpha_m} - (1-\eta_1)\gamma^n, \qquad (1)$$

where $\alpha_m(\alpha_B)$ is the intercept of the leading exchanged meson (baryon) trajectory and $\eta_1(\leq 1)$, $\beta(>1)$ and $\gamma(<1)$ are constants. The first term in Eq. (1) is the annihilation contribution and the above result lends further credence to the hypothesis that annihilations can be estimated from the difference between $\bar{p}p$ and pp when a large number of final states are summed over.

In the same spirit, we can study the rapidity spectra for inclusive $\pi^\pm$ production in $\bar{p}p$, pp and $\bar{p}p$ annihilation processes. Figure 6 shows the laboratory rapidity distributions at 100 GeV/c for $\bar{p}p$ and pp as well as for their difference. There is an indication that the ($\bar{p}p$-pp) data have a central region plateau of 2-3 units, although the statistical errors of the present data sample prohibit any definite conclusion. The transverse momentum distributions $d\sigma/dP_T^2$ (not shown) for π^- (integrated over the backward cm hemisphere) show no significant differences between the $\bar{p}p$ and pp data apart from the overall normalization difference.

II. $\pi^\pm$ production in the target and beam fragmentation regions

Consider the process a+b → c + anything in the kinematic region where c has a small momentum in the rest frame of the target b.

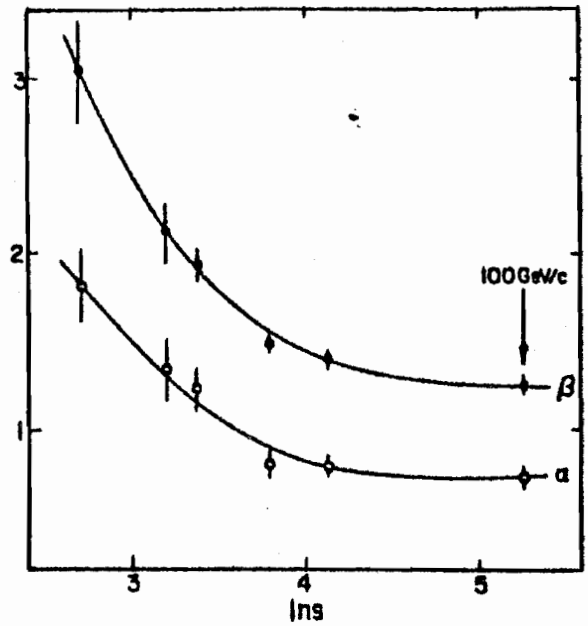

Fig. 5. Values of $\alpha \equiv -\ell nA/\ell ns$ and β obtained from the fits in Figure 4. The curves are to guide the eye.

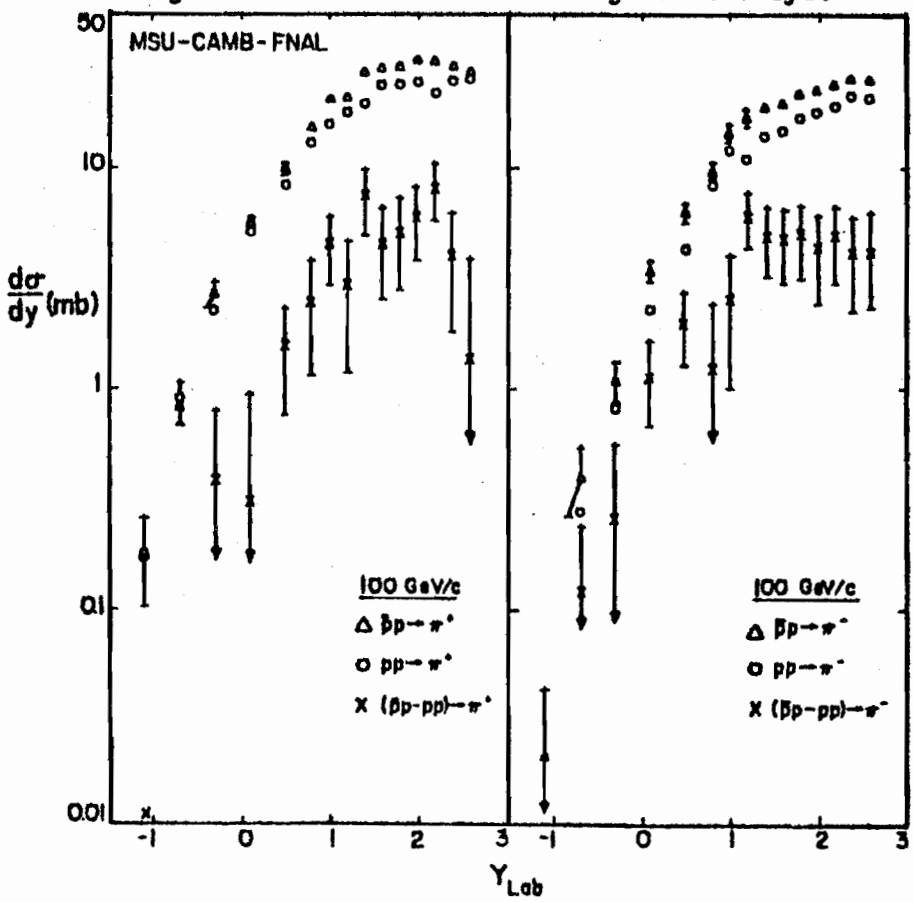

Fig. 6. Laboratory rapidity distributions for $\pi^{\pm}$ production in $\bar{p}p$ and pp interactions. Also shown are the ($\bar{p}p$-pp) differences.

Following[7] Chan Hong-Mo et al., and Miettinen we expect that in this region

$$E\frac{d^3\sigma}{dp^3} = A(P_L, P_T^2) + \sum_M B_M(P_L, P_T^2)s^{-\frac{1}{2}} \qquad (2)$$

where $P_L(P_T)$ is the longitudinal (transverse) momentum of c in the rest frame of b. The first term comes from the Pomeranchuk singularity and the second term arises from the Meson trajectories with t=0 intercept of ½. Since transverse momentum is well known to be limited, we integrate over P_T^2 and study the distribution $G(P_L) = \frac{1}{\sigma_T^{\infty}} \int E\frac{d^3\sigma}{dp^3} dp_T^2$, evaluated in the laboratory. Figure 7 shows this distribution[8] for π^- production in $\pi^\pm p$ and $p^\pm p$ interactions at 100 GeV/c. To a first approximation, all four distributions have the same shape and magnitude, suggesting agreement with the hypothesis of Pomeron factorization. However, on closer examination one observes certain differences, eg. the $\bar{p}p$ data are systematically higher and the π^+p and pp data tend to be lower than the π^-p data. This is shown in more detail in Fig. 8 where the ratio of $G(P_L)$ for $\bar{p}p$, π^+p and pp to π^-p at 100 GeV/c are evaluated as a function of P_L. Also shown are some 200 GeV/c data[8] for pp and π^-p.

To study the energy dependence of these target fragmentation cross sections, distributions such as those shown in Fig. 7 are integrated from $-0.4 \leq P_L \leq 0.2$ GeV/c and plotted[9] as a function of $s^{-\frac{1}{2}}$ in Fig. 9a for π^- and in Fig. 9b for π^+ production for all available reactions. The dominant features are:[9]

a) Most reactions exhibit falling cross sections in disagreement with the hypothesis of limiting fragmentation.

b) However, the approach to a possible scaling behavior in the limit of infinite energy does appear consistent with the expected $s^{-\frac{1}{2}}$ dependence of Eq. (2).

c) Some processes (eg. $\pi^-p \to \pi^-$, $\gamma p \to \pi^-$, $\pi^+p \to \pi^+$) show a rapid decrease with increasing energy. These reactions are characterized by having no exotic combination of particles (ab, $a\bar{c}$, $b\bar{c}$ or $ab\bar{c}$), while other reactions (eg. $\pi^+p \to \pi^-$ and $\pi^-p \to \pi^+$) are less dependent on $s^{-\frac{1}{2}}$ and are characterized by having $a\bar{c}$ exotic. Whether or not these exoticity classifications are the relevant ones will be clarified when more data on $\bar{p}p$ and $K^\pm p$ interactions become available for a wider range of energies.

d) Because of the detailed structure of Eq. (2) for the different processes studied, Fig. 9 does not immediately

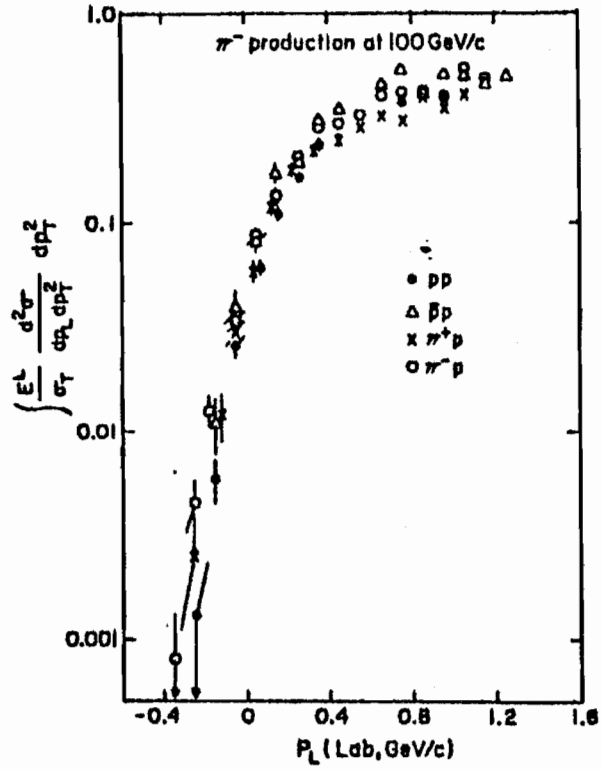

Fig. 7. Distribution of the laboratory longitudinal momentum for π^- production in $\pi^{\pm}p$ and $p^{\pm}p$ interactions at 100 GeV/c.

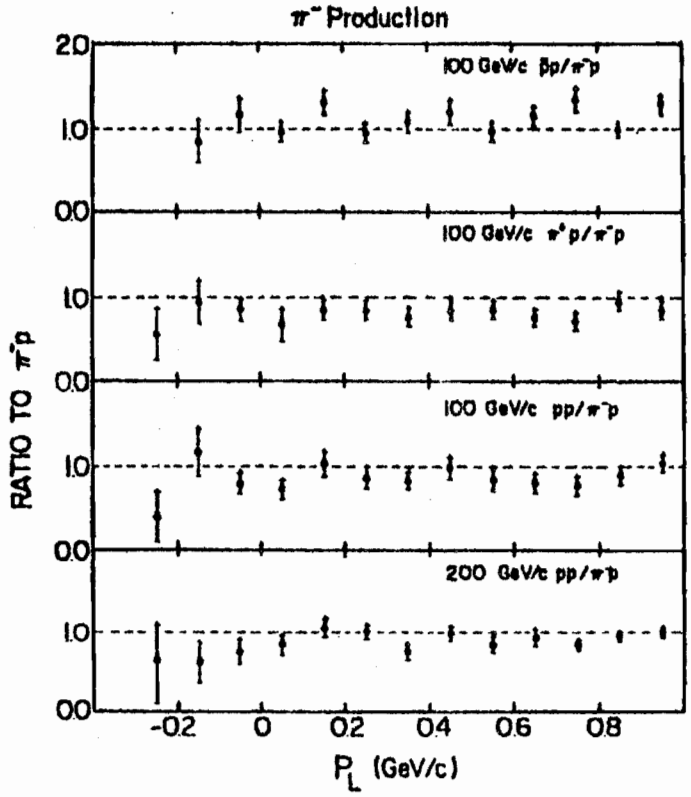

Fig. 8. Ratio of the invariant cross section for π^- production in $\bar{p}p$, π^+p and pp to the π^-p cross section as a function of the laboratory longitudinal momentum.

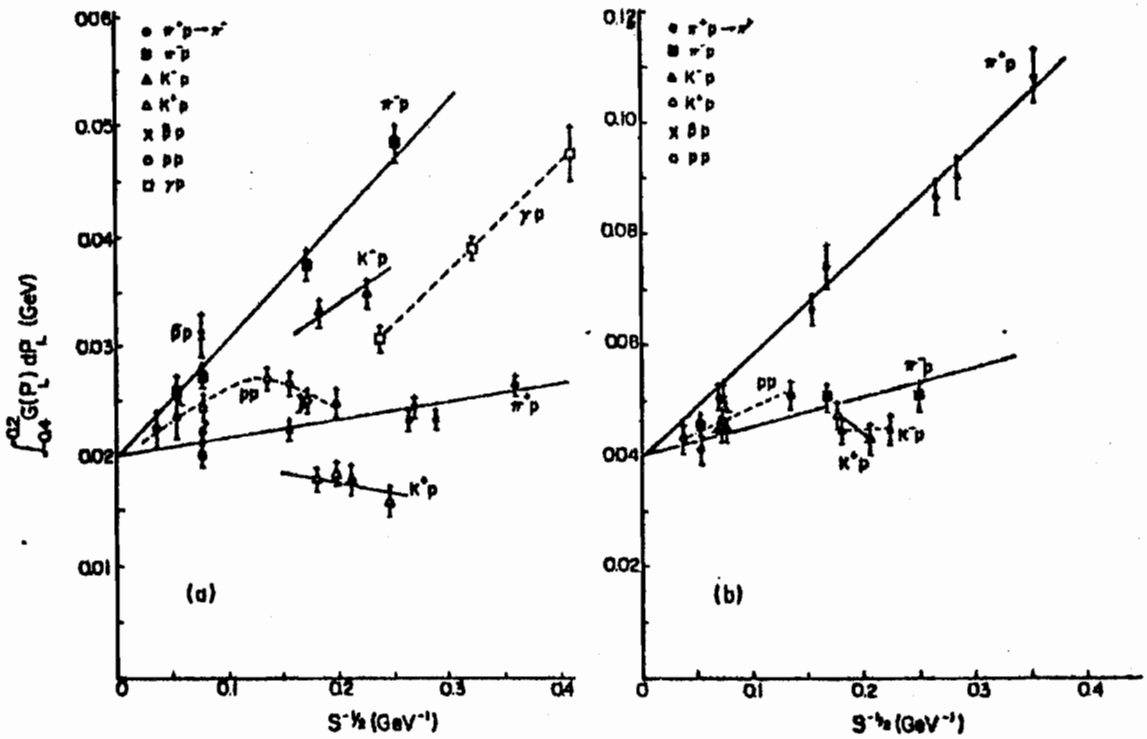

Fig. 9. The invariant cross sections for (a) π^- and (b) π^+ production, integrated over all P_T^2 and $-0.4 < P_L < 0.2$ GeV/c, versus $s^{-1/2}$. The curves are to guide the eye.

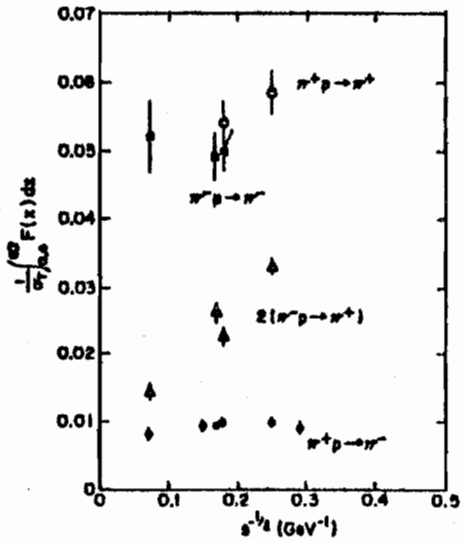

Fig. 10. The invariant cross sections for $\pi^{\pm}p \to \pi$, integrated over all P_T^2 and $x > 0.4$, as a function of $s^{-1/2}$.

confirm or refute the hypothesis of Pomeron factorization. However, the trend of the data for most of the processes shown does suggest that factorization may hold in the limit of infinite energy, i.e., the data appear to converge to a common value as $\sqrt{s} \to \infty$.

A similar analysis can be made for π production in the beam fragmentation region. Due to a lack of data in the most suitable variable, P_L in the rest frame of the beam, the data have been integrated over the region $0.4 \leq x \leq 1$, where $x = P_L^*/P^*_{max} \approx 2P_L^*/\sqrt{s}$. The resulting distributions are shown in Fig. 10 for πp data as a function of $s^{-\frac{1}{2}}$. The $\pi^+p \to \pi^+$ and $\pi^-p \to \pi^-$ are dominated by the diffractive excitation of the target proton, are approximately equal, and show little energy dependence. The other two processes behave in a manner very similar to data in the target fragmentation region i.e., falling with energy and appearing to approach the same value at infinite energy. (Note the factor of 2 multiplying the $\pi^-p \to \pi^+$ data).

III. Leading cluster and ρ° production

In a recent study of π^-p interactions at 205 GeV/c, Yost et. al.[10] have studied peripheral processes in inelastic events and have found that there seems to be a limit to the fraction of incident energy available for particle production. Figure 11a shows[10] the average value of x for the vector sums of the three momenta of all negative and all positive tracks as a function of the associated charged multiplicity. For $n_{ch} \leq 10$, $|\langle x \rangle|$ decreases rapidly with increasing number of produced particles. For $n_{ch} > 10$, however, the data are suggestive of being independent of n_{ch} and motivate the concept of "limiting peripherality."

Figure 11a also shows clearly that the leading particle effect (LPE) persists to high multiplicities, since $\langle x \rangle > 0$ for negative particles and $\langle x \rangle < 0$ for positive particles even for $n_{ch} = 18$. A measure of the rapidity range of this LPE is shown in Fig. 11b and 11c where $f_b(f_t)$ is the fraction of events in which the highest (lowest) rapidity charged particle is negative. The lines of $f_b = f_t = 0.5$ represent no charge preference. Since the leading particles tend to have the sign of the beam (or target), we observe that the LPE is maintained over a range of about 2 rapidity units, in good agreement with previous estimates of the range of a cluster's decay products.

Recently, there have been several studies of inclusive resonance production, in particular, ρ° production. Figure 12 shows an example of inclusive ρ° production at low ($\leq$ 20 GeV/c) energy.[11] Figure 12(a) to (e) shows the $(\pi^+\pi^-)$ mass distribution for fixed

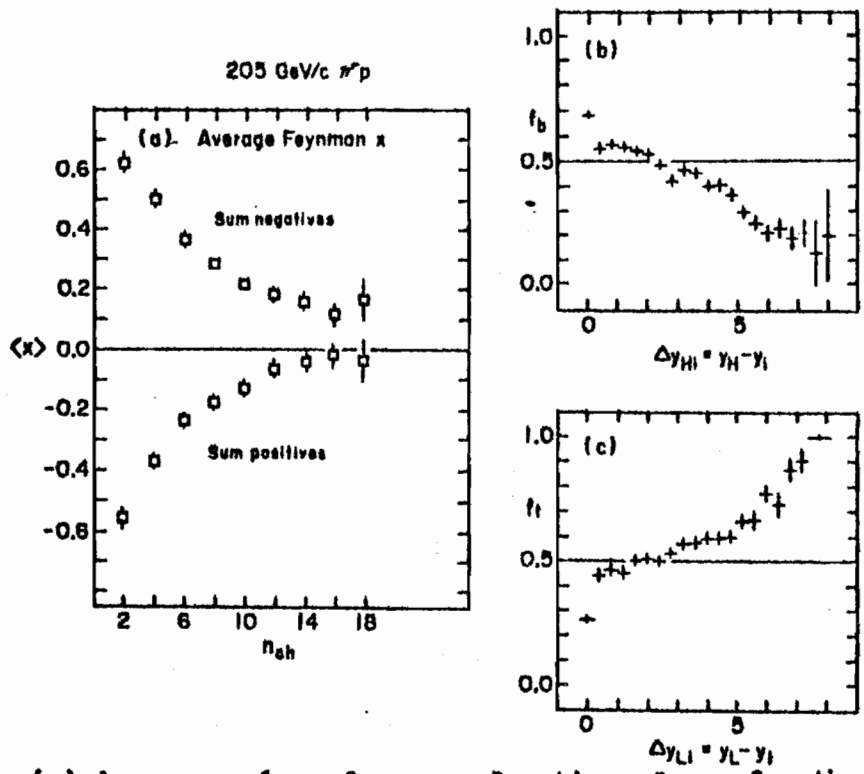

Fig. 11. (a) Average value of x as a function of n_{ch} for the sum of all negative and of all positive tracks. (b) The inclusive average probability of negative particle emission f_b as a function of Δy_{Hi}. (c) Same as (b), but for f_t versus Δy_{Li}.

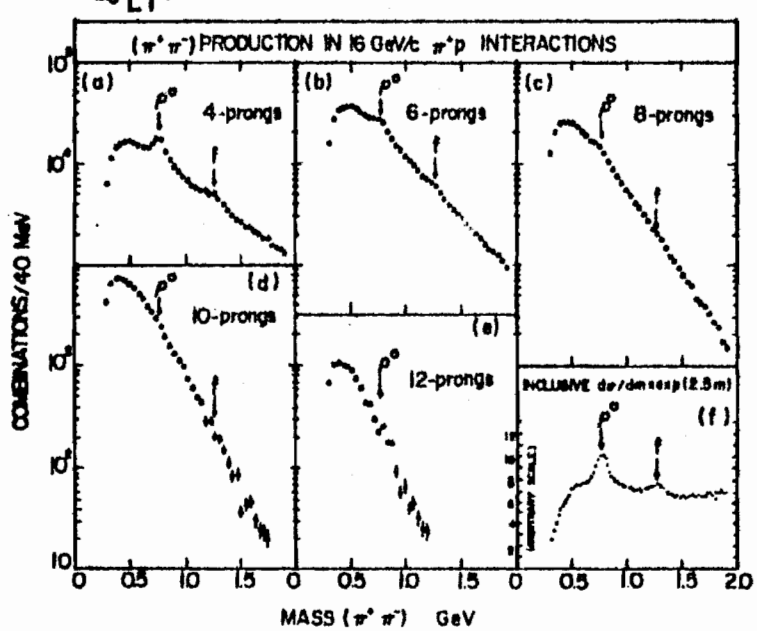

Fig. 12. (a) to (e) Mass spectra for semi-inclusive $\pi^+\pi^-$ production. (f) inclusive mass spectrum multiplied by exp (2.5m).

charged multiplicity. Clear ρ° peaks are observable in the 4, 6 and 8 prongs and clear f peaks in the 4 and 6 prongs. The inclusive ρ° and f peaks are more clearly observed after multiplying the $\pi^+\pi^-$ mass spectrum by $e^{2.5m}$ as shown in Fig. 12(f).

Figure 13 shows the results of a recent study[12] of ρ° production in 205 GeV/c pp interactions. The inclusive $\pi^+\pi^-$ spectrum (Fig. 13a) shows a clear ρ° signal. The semi-inclusive distributions indicate no ρ° signal in the 4 prongs (not shown) nor in 12-18 prong events. Strong resonance production is confined to the 6-10 prongs where there are (0.25 ± 0.10) ρ°'s per event. Figure 13(b) shows the inclusive $\pi^+\pi^-$ mass spectrum for different cuts on the rapidity of the $\pi\pi$ system. For $|y_{\pi\pi}| > 2.0$ there is little ρ° production, while almost 2/3 of all ρ°'s are produced for $|y_{\pi\pi}| < 1$.

Figure 14 shows a summary of ρ° production in $\pi^\pm p$ and pp interactions from 6 to 205 GeV/c. The total inclusive ρ° cross section is seen to rise by a factor of ~3 in this energy range. This increase is comparable to that observed in π production as shown in Fig. 14 where the ratio of ρ°/π^-, plotted versus the incident laboratory momentum, shows little variation over the 6-205 GeV/c range. It is interesting to note that this ratio is twice as large in πp interactions as in pp collisions. This difference comes mainly from the forward ρ° production in the π dissociation cm hemisphere.

IV. Exclusive reactions at 100-300 GeV/c

The exclusive reactions

$$\pi^- p \rightarrow \pi^- p \pi^+ \pi^- \qquad (3)$$

and

$$\pi^- p \rightarrow \pi^- p 2\pi^+ 2\pi^- \qquad (4)$$

at 100 GeV/c, and

$$pp \rightarrow pp\pi^+\pi^- \qquad (5)$$

and

$$pp \rightarrow pp2\pi^+2\pi^- \qquad (6)$$

at 200 and 300 GeV/c are currently being studied by the MSU-ANL-Fermilab-ISU-Md collaboration. At the present time only preliminary results are available and are based on approximately one-half the data in existing film. In Table I we give the measured cross sections for reactions (3-6). The values for reactions (3) and (5) agree well with previous results in this energy range. The new results for (4) and (6) represent the first measurements of these reactions above 28.5 GeV/c and are shown in Fig. 15 as a function of the incident momentum. The following discussion centers on two currently interesting topics, namely Double Pomeron Exchange and Double Diffractive Excitation.

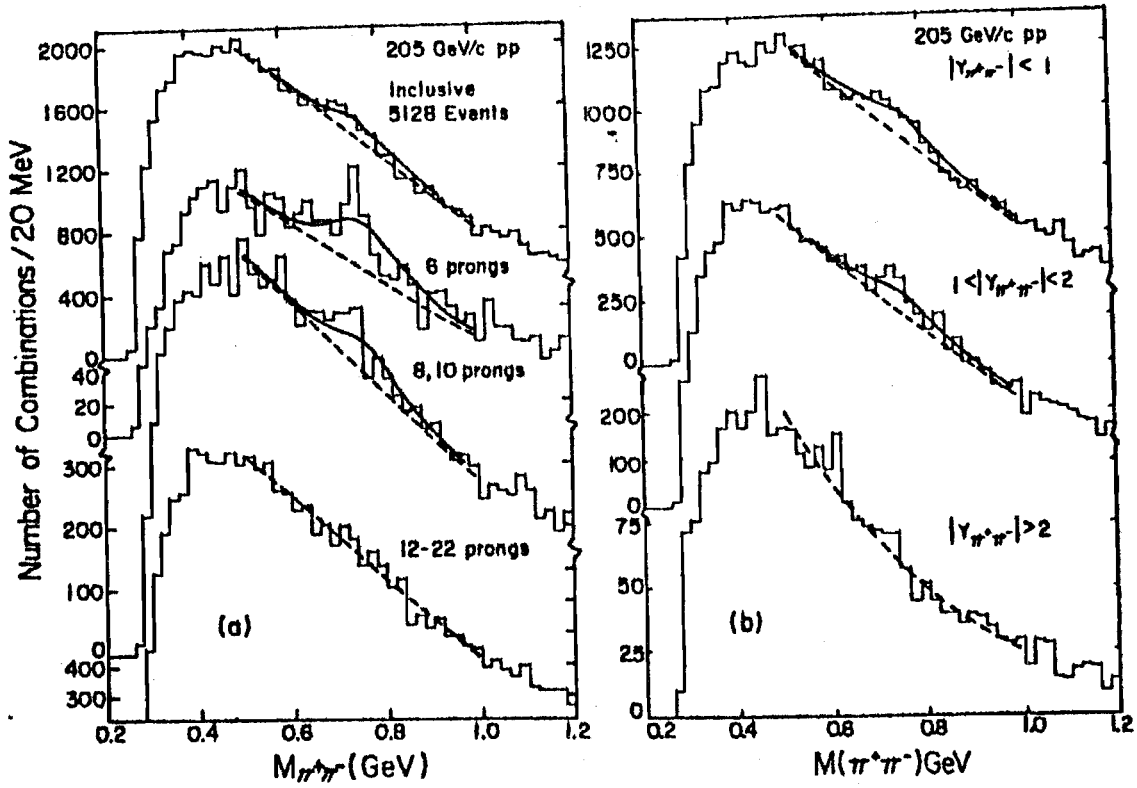

Fig. 13. (a)Inclusive and semi-inclusive mass spectra for $\pi^+\pi^-$ production in 205 GeV/c pp interactions. (b) Inclusive mass spectra for various $\pi^+\pi^-$ rapidity intervals.

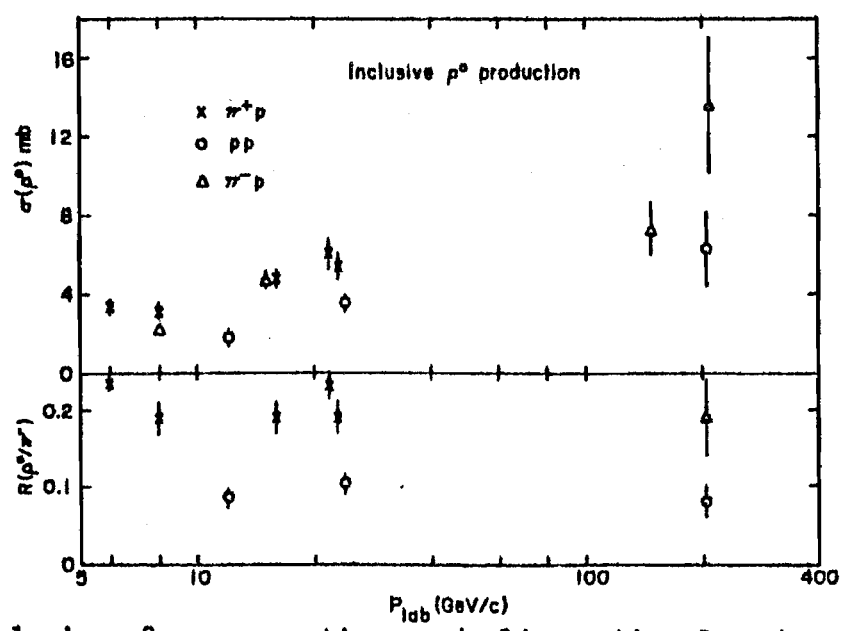

Fig. 14. Inclusive ρ^0 cross sections and ρ^0/π^- ratios for $\pi^\pm p$ and pp data as a function of the incident beam momentum.

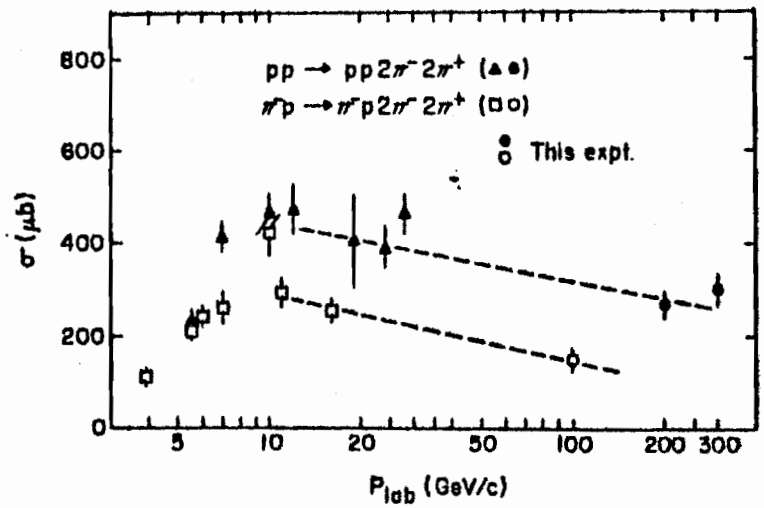

Fig. 15. Cross sections for the 6-body final states in π^-p and pp interactions versus the incident beam momentum.

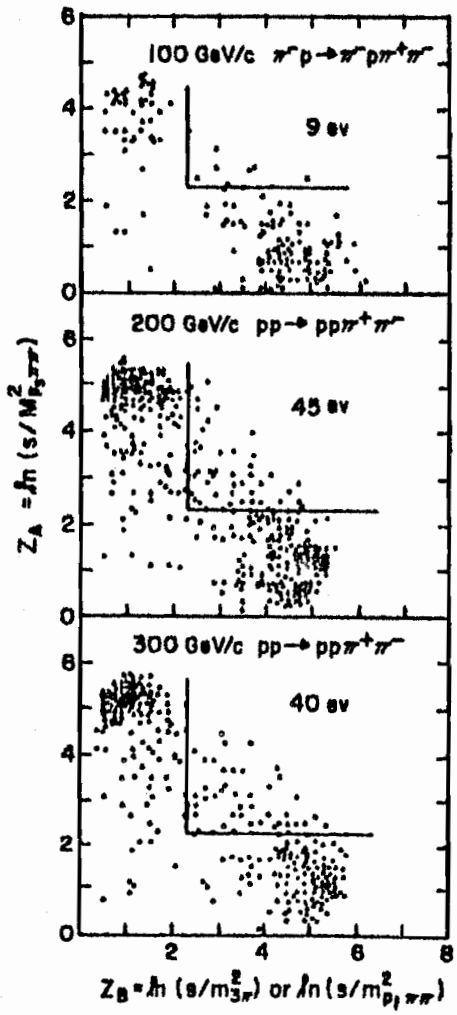

Fig. 16. Z_A versus Z_B for the exclusive 4-body final states.

Table I

Exclusive Channel Results

Beam	Events Analyzed	4c events	Reaction	$\sigma(\mu b)$
100 GeV/c	1117	141	(3)	600 ± 50
$\pi^- p$	1297	37	(4)	150 ± 30
200 GeV/c	3032	354	(5)	690 ± 50
pp	3173	124	(6)	270 ± 30
300 GeV/c	2024	256	(5)	640 ± 50
pp	2365	121	(6)	300 ± 30

a) Double Pomeron Exchange (DPE)

Following the work of Chew and Chew,[13] in Fig. 16 we plot Z_A versus Z_B($Z_A = \ln(s/M^2(p_s\pi^+\pi^-))$, $Z_B = \ln(s/M^2(p_f\pi^+\pi^-))$) for reactions (3) and (5). The criterion[13] that Z_A, $Z_B > 2.3$ defines a possible DPE sample of 85 events (for the combined 200 and 300 GeV/c pp data). Since it is possible that a background from the "tails" of single diffraction (SD) could exist in this region of phase space, we show in Fig. 17(a) the distribution of ϕ, the azimuthal angle between the transverse momentum vectors of the two protons in reaction (5), for the total sample as well as for the 85 DPE candidates. If the Pomeranchuk singularity is a simple pole without any Regge cut contributions, then the azimuthal distribution for DPE should be isotropic. We attribute the excess of events near $|\phi| = \pi$ to an SD tail. Evidence for this is shown in Fig. 17(b) where ϕ is plotted as a function of the $p\pi^+\pi^-$ mass for the DPE candidates. It is clear that the excess near $\phi = \pi$ is due to events with low $p\pi^+\pi^-$ mass. After selecting $M(p\pi^+\pi^-) > 2.8$ GeV, we find 65 events corresponding to a DPE cross section of $(62\pm11)\mu b$. This result is shown in Fig. 18 and is in good agreement with the prediction of Chew and Chew.[13]

b) Double Diffractive Excitation (DDE)

Data from reaction (6) may be used to study the possible existence of the simultaneous diffraction of target and beam protons into the $p\pi^+\pi^-$ final state and hence a comparison with the predictions of Pomeron factorization based on data from reaction (5). The $p\pi^+\pi^-$ mass spectrum for the 4 body final state is shown in Fig. 19(a) for all events and for those events with 3 particles in one cm hemisphere and one in the other (3:1 configuration). A strong 1700 MeV mass peak is visible as well as a possible shoulder around 1500 MeV. For comparison Fig. 19(b) shows the $p\pi^+\pi^-$ mass

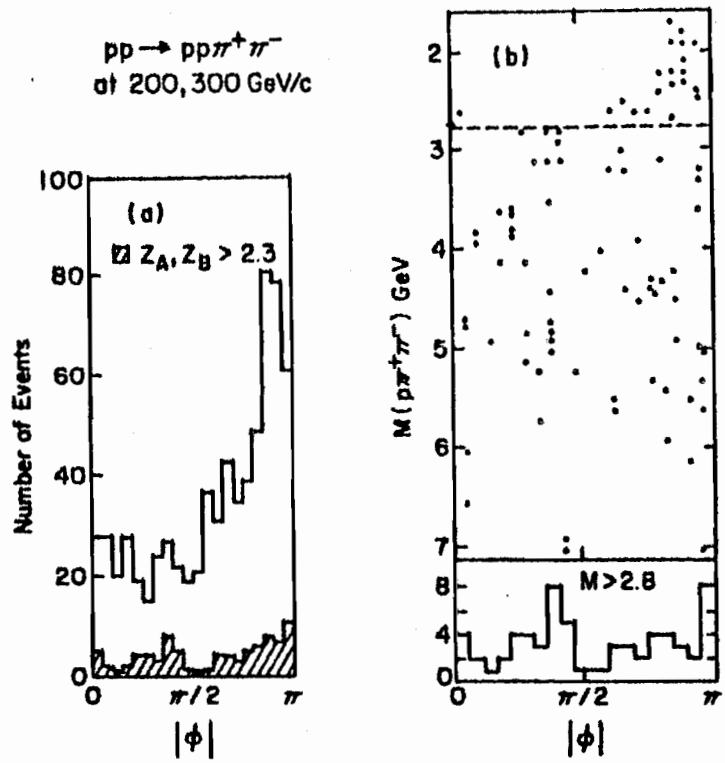

Fig. 17. (a) The distribution for the difference in azimuth angle of the two protons in $pp \to pp\pi^+\pi^-$. (b) The azimuthal angular distribution versus the $p\pi^+\pi^-$ mass.

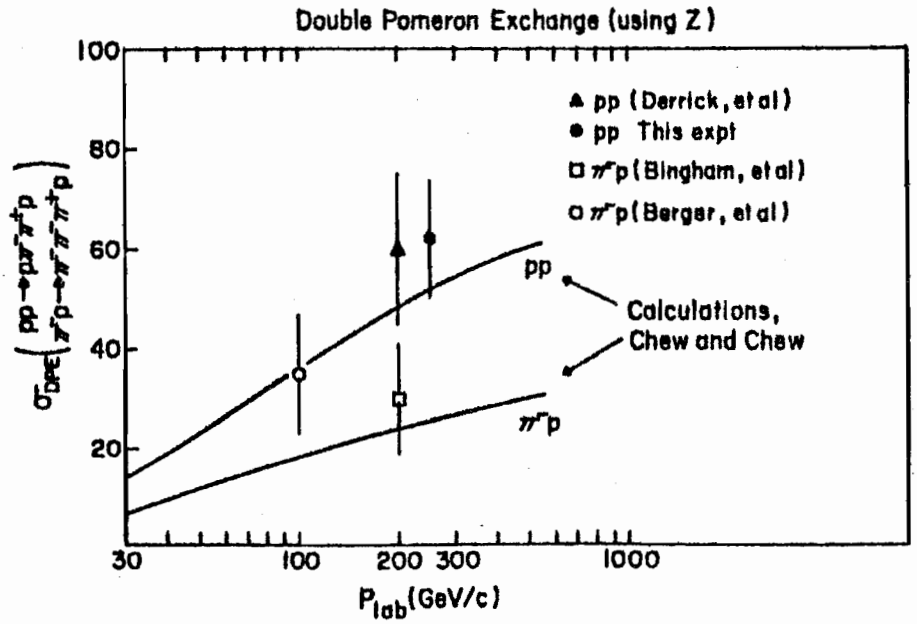

Fig. 18. Momentum dependence of the Double Pomeron exchange contribution to the exclusive 4-body final state.

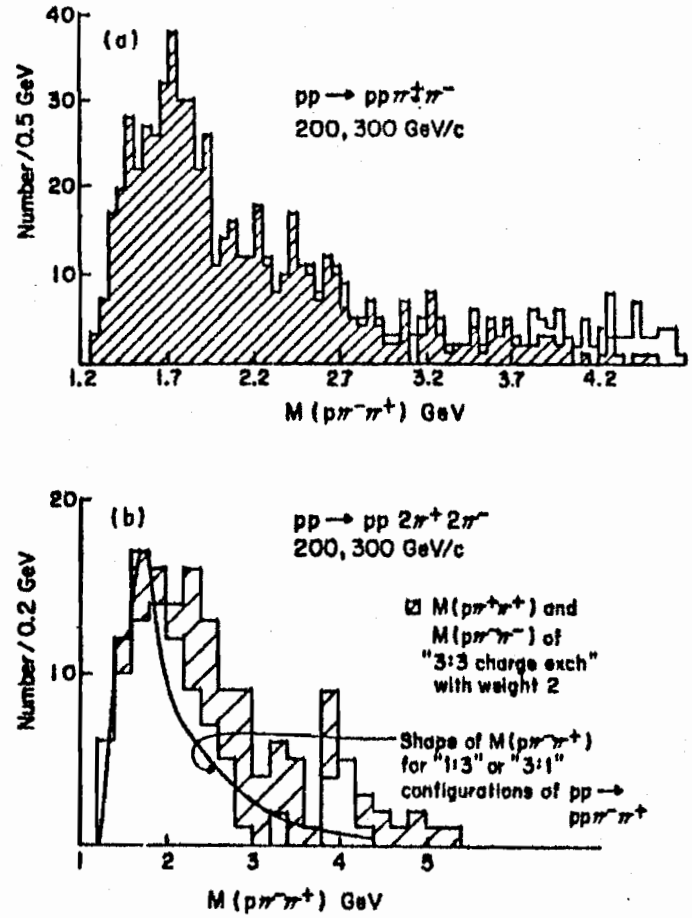

Fig. 19. The $p\pi^+\pi^-$ mass spectrum for (a) the $pp\pi^+\pi^-$ and (b) the $pp2\pi^+2\pi^-$ final state.

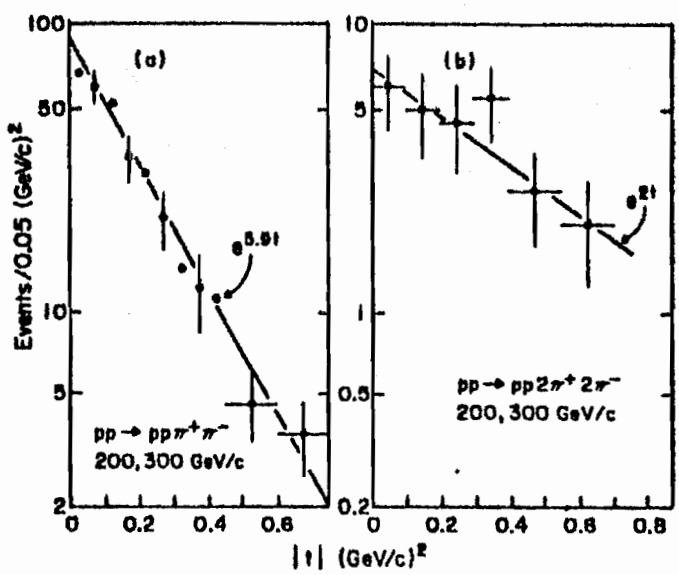

Fig. 20. t distributions for the $p\pi^+\pi^-$ system in (a) the $pp\pi^+\pi^-$ and (b) the $pp2\pi^+2\pi^-$ final state.

distribution for reaction (6) for events of the 3:3 no charge exchange configuration. To remove "background" due to high mass SD, we make a subtraction based on the 3:3 configuration in which there is apparent charge exchange between cm hemispheres. The resulting spectrum is then in excellent agreement with that observed in Fig. 19(a). Figure 20 shows the t distribution (a) for SD in reaction (5) and (b) for DDE in reaction (6). We observe a much flatter t distribution for DDE than for SD. (Note that these distributions are integrated over the same mass spectra - Fig. 19.)

Finally we test the hypothesis of factorization:

$$\frac{d\sigma}{dt}(p_1{*}p_2{*}) = \frac{d\sigma}{dt}(p_1{*}p_2)\,\frac{d\sigma}{dt}(p_1p_2{*})/\frac{d\sigma}{dt}(\text{elast}).$$

If we use integrated cross sections and assume an e^{bt} dependence (Fig. 20), then

$$\sigma_{p_1{*}p_2{*}} = (\sigma_{p_1{*}p_2}\cdot\sigma_{p_1p_2{*}}/\sigma_{el})(b_{p_1{*}p_2}\cdot b_{p_1p_2{*}}/b_{p_1{*}p_2{*}}\cdot b_{el}), \quad (7)$$

and $$b_{p_1{*}p_2{*}} = b_{p_1{*}p_2} + b_{p_1p_2{*}} - b_{el}. \quad (8)$$

From Fig. 20, we find that LHS (8) = 2.0 ± 0.5 $(\text{GeV/c})^{-2}$ and that RHS (8) = 2.5 ± 0.6 $(\text{GeV/c})^{-2}$. As a test of Eq. (7), we predict (RHS) that $\sigma_{p_1{*}p_2{*}}$ = 23 ± 7 μb, while experimentally we observe $\sigma_{p_1{*}p_2{*}}$ = 37 ± 10 μb. Taking the ratio of these cross sections we find $\sigma_{exp}/\sigma_{pred}$ = 1.6 ± 0.7. On the basis of these data we conclude that we have seen DDE and that we have no evidence for a violation of Pomeron factorization.

ACKNOWLEDGMENTS

It is a pleasure to thank my colleagues, B. Y. Oh, D. L. Parker and G. A. Smith, for their contributions to the data presented in this report.

REFERENCES

*Work supported in part by the National Science Foundation

1. R. E. Ansorge et al., "Charged Particle Multiplicities in 100 GeV/c $\bar{p}p$ Interactions," to be published (1975).

2. J. Whitmore et al., Proceedings of the IVth International Antinucleon-Nucleon Symposium, Syracuse (1975).

3. A. S. Carroll et al., FERMILAB-Pub. 75/51-EXP. (1975).

4. J. G. Rushbrooke et al., "On the Difference Between $\bar{p}p$ and pp Topological Cross Sections up to 100 GeV/c," to be published (1975).

5. T. Fields et al., Proceedings of the IIIrd International Antinucleon-Nucleon Symposium, Liblice, Prague (1974).

6. Y. Eylon and H. Harari, Nucl. Phys. B80, 349 (1974).

7. Chan Hong-Mo, et al., Phys. Rev. Lett. 26, 672 (1971); H. I. Miettinen, Phys. Letters 38B, 431 (1972).

8. Private communication from C. Bromberg, W. Ko, R. Singer and the Wide-Gap Spark Chamber Hybrid Collaboration.

9. J. Whitmore et al., "Approach to Scaling and Factorization in Proton Fragmentation Into $\pi^{\pm}$," to be submitted for publication (1975).

10. G. P. Yost et al., "Leading Particles in π^-p Interactions at 205 GeV/c," submitted for publication (1975).

11. M. Deutschmann et al., CERN/D.Ph.II/PHYS 75-29 (1975).

12. R. Singer et al., "ρ^0 Production in 205 GeV/c pp Interactions," ANL-HEP-PR-75-48 (1975).

13. D. M. Chew and G. F. Chew, Phys. Lett., 53B, 191 (1974).